SUPPORTING INFORMATION

Hyperbranched Quasi-1D TiO_2 Nanostructure for Hybrid Organic-Inorganic Solar Cells

Ali Ghadirzadeh,[a,b] Luca Passoni,[a,c] Giulia Grancini,[a] Giancarlo Terraneo,[d] Andrea Li Bassi,[a,b] Annamaria Petrozza,[a] Fabio Di Fonzo[a*]

[a] *Center for Nanoscience and Technology @PoliMi, Istituto Italiano di Tecnologia, Via Pascoli 70/3, 20133 Milano, Italy*

[b] *Politecnico di Milano, Dip.to di Energia, Via Ponzio, 20133 Milano, Italy*

[c] *Politecnico di Milano, Dip.to di Fisica, P.zza L. Da Vinci 32, 20133 Milano, Italy*

[d] *Laboratory of Nanostructured Fluorinated Materials (NFMLab), Department of Chemistry, Materials, and Chemical Engineering "Giulio Natta", Politecnico di Milano, Milan, Italy*

*Corresponding Author: Fabio Di Fonzo. Email: fabio.difonzo@iit.it Tel. +39 0223999868

Comparative table of different devices performance in the field of organic-inorganic hybrid solar cells:

Base	System	Jsc (mA/cm^2)	Voc (V)	FF	PCE (%)	Ref.
TCO/TiO_2/P3HT systems						
Nanoparticles	TiO_2/P3HT	1.4	0.72	0.51	0.45*	1
Nanotube	TiO_2/P3HT	1.8	0.62	0.58	0.5	2
Nanorod	TiO_2/P3HT	2.73	0.64	0.56	0.98	3
More complex systems						
Nanorod	TiO_2/dye/P3HT	4.33	0.78	0.65	2.2	4
Nanoparticles	TiO_2/dye/P3HT	4.71	0.87	0.68	2.81	5
Nanotube	FTO/PEDOT:PSS/P3HT:PCBM/TiO_2	3.91	0.51	0.43	4.18	6
Reference						
Nanoparticles	TiO_2/P3HT	1.4	0.51	0.50	0.37	9

**Extrapolated from EQE measurements*

Table S1. Performance comparison of different devices.

Methods

Material fabrication

Photoanodes are fabricated on FTO glass (Dyesol, 15 Ωsq^{-1})A 100 nm thick titania blocking layer was deposited on all substrates by spray pyrolysis of a 1:10 mixture of titanium diisopropoxide by Sigma Aldrich, 75 wt. % in isopropanol with ethanol by Sigma-Adrich, 99.8% purity, on hotplate at 500^{o}CHyperbranched nanostructures are grown by pulsed laser deposition (PLD) where a KrF excimer laser with (λ=248 nm and energy density of 2.5 Jcm^{-2}) operating at 20 Hz ablates a target of TiO_2 (purity of 99.99%, Testbourne). Sample to target distance was 5 cm and the samples rotate to achieve higher film uniformity (linear velocity of ~1 m/s). As-deposited samples were annealed at 500 ^{o}C for two hours. Control porous films of titanium dioxide nanoparticles was prepared by doctor blading standard ethanol-diluted 18NR-T titania paste by DyeSol, and annealed 500 ^{o}C for 45 minutes was used as a reference. Both photoanodes are treated in 0.5 mM $TiCl_4$ solution in deionized H_2O at 70^{o}C for one hour. Samples were washed in deionized water and finally annealed again at 550^{o}C for 45 minutes.

Device fabrication

Hybrid devices were fabricated by two step spin-coating (5 seconds idle and 1 minute at 1000 rpm) of a 30 g/L solution of P3HT (20K region-regular, lisicon 001 by Merck) in Chlorobenzene (99.9% purity by Sigma-Aldrich). To obtain crystalline polymer film, samples are annealed at 144^{o}C for 20 minutes in an inert N_2 atmosphere. Finally, a 200 nm silver film is evaporated as cathodic contact with a MBRAUN thermal evaporator

J-V characterization

A Newport Sun Simulator (Oriel Sol3A Class AAA) with solar spectrum AM 1.5 is used to measure the photovoltaic performance and power conversion efficiency of the cells. Sun Simulator was previously calibrated in intensity with a NREL certified Oriel Si reference cell. For the spectral measurement, a 45W quartz-tungsten-halogen lamp from Newport was used to account for attenuation in the measurement system (at 1 sun the mismatch factor was found to be 0.994).

Material characterization

Optical characterization is carried out by a UV/Vis spectrophotometer (Perkin-Elmer lambda 1050 spectrophotometer-Xe lamp). An integrating sphere was used for the measurements in order to include the transmitted scattered light in the absorption calculation.

X-ray powder diffraction experiments are carried out on a Bruker D8 Advance diffractometer operating in reflection mode with Ge-monochromated Cu Kα1 radiation (λ = 1.5406 Å) and a linear position-sensitive detector, with a 2θ range of 20-80° and a step size of 0.016°.

Crystallinity of polymer inside the photoanodes is also studied by nanosecond transient absorption measurements. The technique is based on a standard *pump-probe* setup where the sample is excited by a nanosecond laser pulse (pump) and the time evolution of the differential absorption changes induced by the pump is monitored by a second weak probe generated by a *CW* light source. The pump pulses are provided by a nanosecond tunable OPOLett-355II laser (10 Hz repetition rate). The probe light is provided by a pulsed Xenon arc lamp. The sample was kept at a 45° angle to the excitation beam. The beams are focused onto the sample ensuring spatial overlap. The transmitted probe is spectrally filtered by a monochromator and detected. Two different detection systems are used: a cooled ICCD camera which enables to detect the entire spectral range from 350 to 850 nm at once and a set of photomultipliers (with both VIS and near-IR detection window) enabling the collection of single-wavelength kinetics with high sensitivity. The signal is finally recorded by a TDS 3032C digital signal analyzer. From the transmission change following photoexcitation the variation in the absorption is thus derived as:

$$\Delta OD(\tau,\lambda)=\log\left(I_{probe}\right)/\left(I_t\left(\tau,\lambda\right)\right)$$

where I_{probe} is the transmitted probe with excitation off and I_t is the transmitted probe after laser excitation. The system has sensitivity of $5 \cdot 10^{-4}$ and a temporal resolution of 7 ns.

Figure S1 show the optical transmittance for the TiO_2/P3HT films for nanostructures with different porosities.

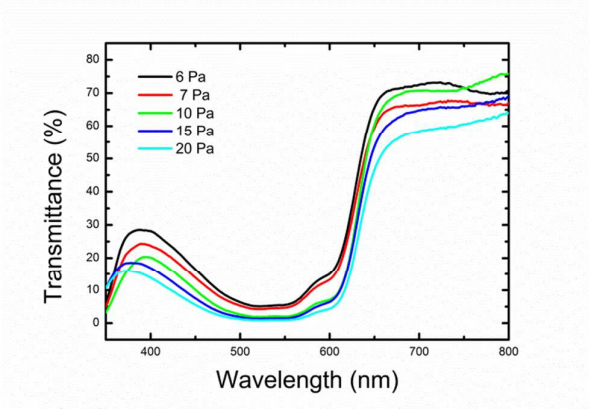

Figure S1. Total transmittance for TiO_2:P3HT pair for different porosity of the titania

In Figures S2 power conversion efficiency, short circuit current, fill factor, and open circuit voltage for thickness optimization are presented together with the average and best device performance of the control samples.

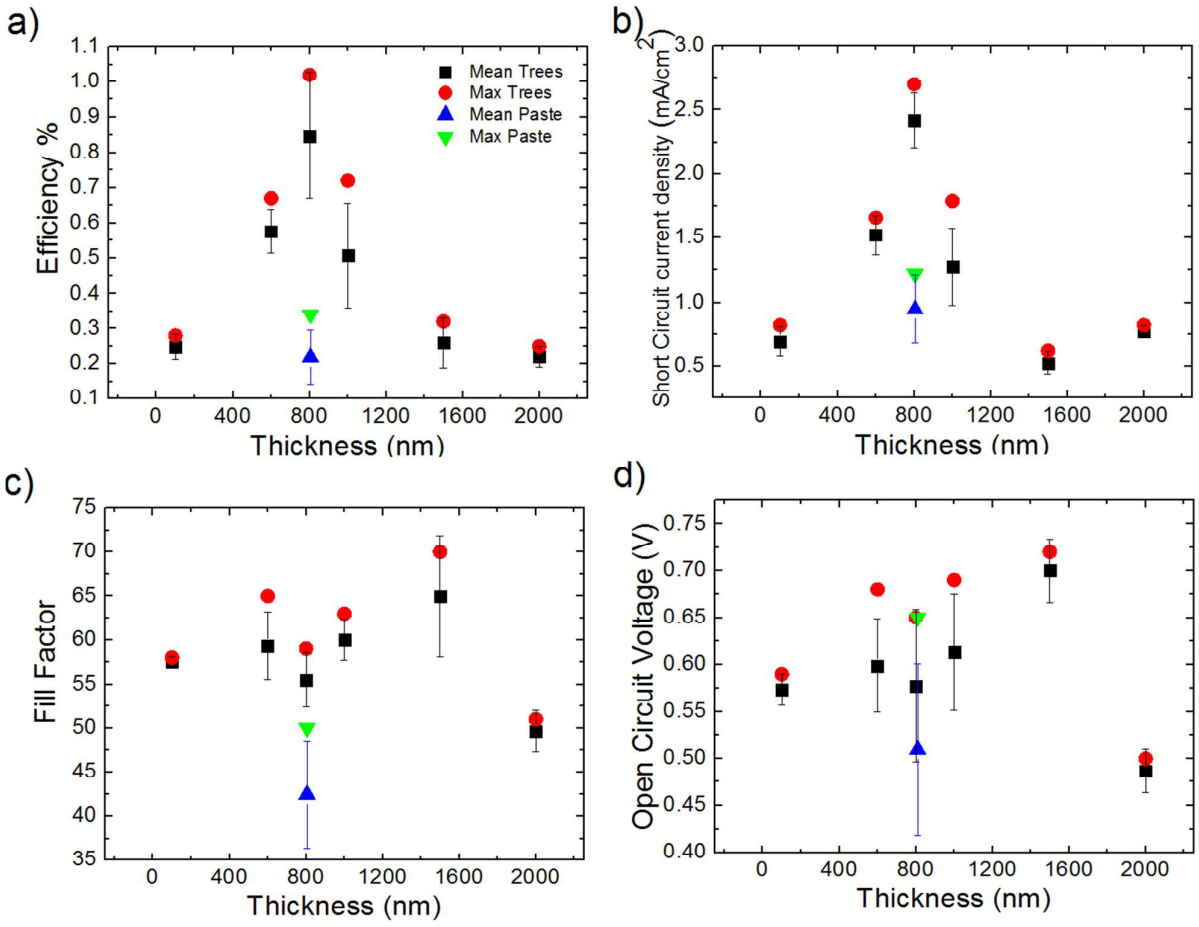

Figure S2. a) Power conversion efficiency, b) short circuit current density, c) fill factor, and d) open circuit voltage for hyperbranched samples with different thicknesses and for the control device with the same thickness of the most performing device.

Figure S3 shows the series resistance for the cells with different thickness. The resistance is calculated by the inverse slope of J-V curve, J=0.

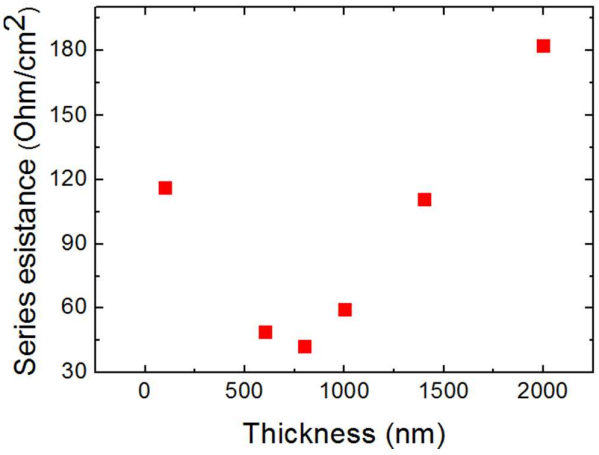

Figure S3. Series resistance as function of film thickness.

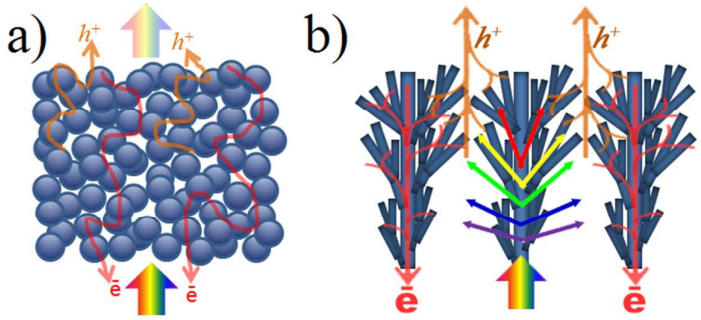

Figure S4 Schematic illustration of structural comparison between (a) the mesoporous structure and (b) the hyperbranched nanostructure.

In Figure S4 a schematic of two nanostructures forming the device photoanode show the main advantaged of the hyperbranched nanostructures. As other highly interconnected hierarchical nanostructures,[7, 8] PLD hyperbranched nanostructures share the light scattering capability, the high specific surface area and the high crystals connectivity. Moreover the directionality of the 1D nanostructures offer preferential pathways for charge collection.

In Figure S5 total transmittance and haze factor of the photoanodes are depicted. The haze factor which is defined as the diffusive over total transmittance is plotted as a function of incident light wavelength, verifying 20 to 60 percent scattering of the transmitted light in the visible region by the hierarchical nanostructure. While the mesoporous structure shows only 7 to 12 percentage.

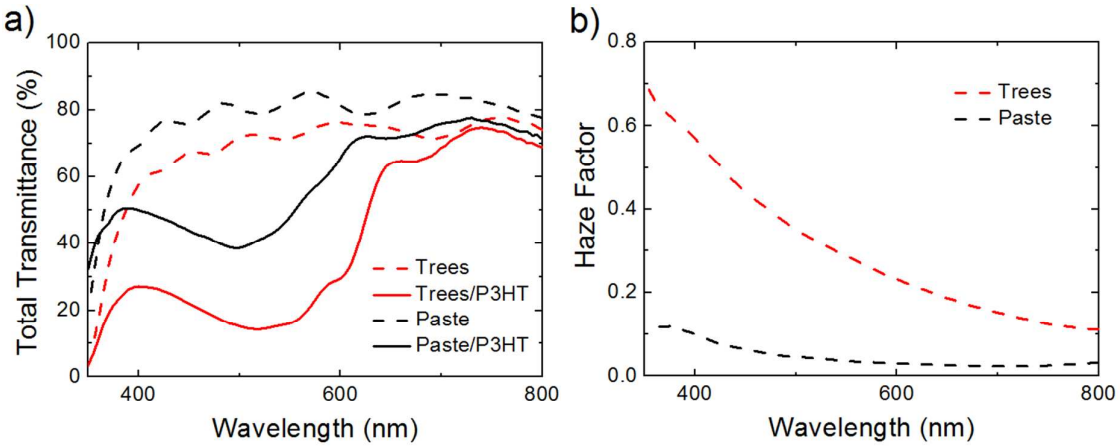

Figure S5. Haze factor for the hierarchical structure and the mesoporous one.

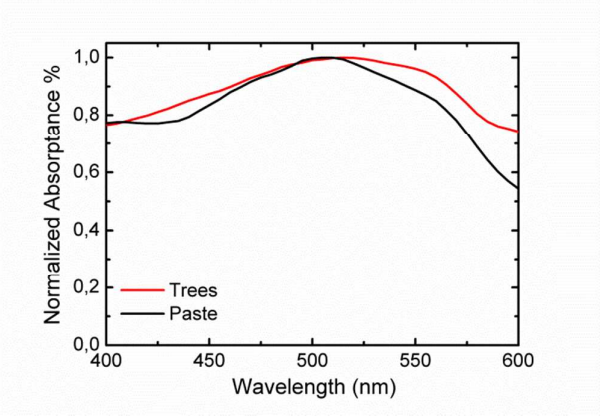

Figure S6. Normalized absorptance highlighting different feature in the absorptance of the hyperbranced nanostructure (red) when compared to that of standard mesoporous devices.

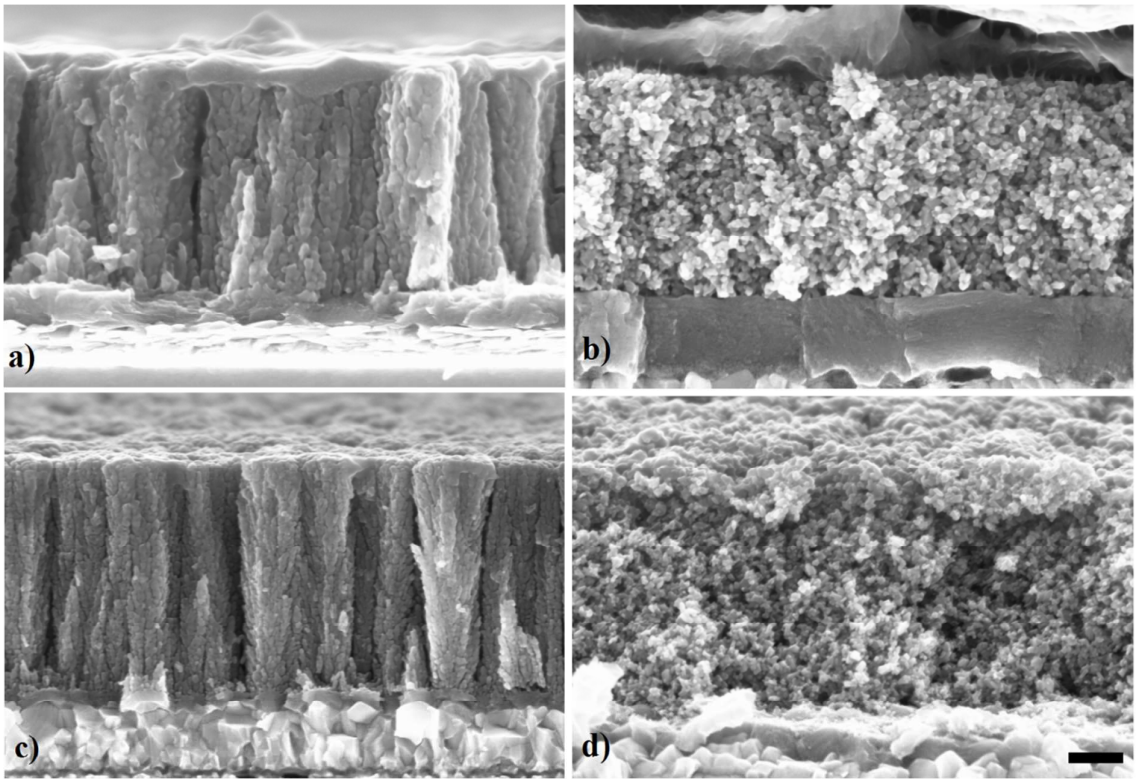

Figure S7. Cross section SEM images (a) PLD samples and (b) nanoparticles paste with capping layer and (c) PLD samples and (d) nanoparticles paste without capping layer used for XRD and nanosecond transient absorption measurements. Scale bar: 100 nm.

References

1. Coakley, K.M.; McGehee, M.D. Photovoltaic Cells Made From Conjugated Polymers Infiltrated Into Mesoporous Titania. Appl. Phys. Lett. **2003,** *83*, 3380-3382.
2. Abrusci, A.; Ding, I. K.; Al-Hashimi, M.; Segal-Peretz, T.; McGehee, M. D.; Heeney, M.; Frey, G. L.; Snaith, H. J. Facile Infiltration of Semiconducting Polymer into Mesoporous Electrodes For Hybrid Solar Cells. Energy Environ. Sci. **2011**, *4,* 3051-3058.
3. Wu, M.-C. *et al.* Nanoscale Morphology and Performance of Molecular-Weight-Dependent Poly(3-Hexylthiophene)/TiO_2 Nanorod Hybrid Solar Cells. J. Mater. Chem. **2008,** *18,* 4097-4102.
4. Lin, Y.-Y.; Chu, T.-H.; Li, S.-S.; Chuang, C.-H.; Chang, C.-H.; Su, W.-F.; Chang, C.-P.; Chu, M.-W.; Chen, C.-W. Interfacial Nanostructuring on the Performance of Polymer/TiO_2 Nanorod Bulk Heterojunction Solar Cells. J. Am. Chem. Soc. **2009**, *131,* 3644-3649.
5. J.Lee, J. Y. J., Fabrication of Highly Ordered and Vertically Oriented TiO_2 Nanotube Arrays for Ordered Heterojunction Polymer/Inorganic Hybrid Solar Cell. Sol. Energy Mater. Sol. Cells **2011,** *95,* 3152–3156.
6. Shankar, K. M., G.K.; Paulose, M.; Varghese, O.K.; Grimes, C.A. Effect of Device Geometry on the Performance of TiO_2 Nanotube Array-Organic Semiconductor Double Heterojunction Solar Cells. J. Non-Cryst. Solids **2008,** *354*, 2767–2771.
7. Lin, J.; Heo, Y.-U.; Nattestad, A.; Yamauchi, Y.; Dou, S. X.; Kim, J. H. Mesoporous Hierarchical Anatase for Dye-sensitized Solar Cells Achieving Over 10% Conversion Efficiency Electrochim. Acta **2015,** *153,* 393-398.

8. Lin, J.; Nattestad, A.; Yu, H.; Bai, Y.; Wang, L.; Dou, S. X.; Kim, J. H. Highly Connected Hierarchical Textured TiO_2 Spheres as Photoanodes for Dye-Sensitized Solar Cells. J. Mater. Chem. A **2014**, *2,* 8902-8909.
9. Canesi, E. V.; Binda, M.; Abate, A.; Guarnera, S.; Moretti, L.; D'Innocenzo, V.; Sai Santosh Kumar, R.; Bertarelli, C.; Abrusci, A.; Snaith, H.; *et al.* The Effect Of Selective Interactions at the Interface of Polymer-Oxide Hybrid Solar Cells. *Energy Environ. Sci.* **2012,** *5*, 9068-9076.